Algorithms for Airborne Ionospheric Front Detection in LAAS Using Carrier Phase and INS Measurements

L. Gratton, F. Chan and B. Pervan, *Illinois Institute of Technology*

ABSTRACT

The Federal Aviation Administration is currently developing the Local Area Augmentation System (LAAS) to transition from the current instrument landing system to satellite based navigation. Due to the single frequency nature of the current LAAS architecture, spatial ionospheric decorrelation contributes significantly to the differential ranging error. During days of normal ionospheric activity, the LAAS Ground Facility (LGF) broadcasts a conservative standard deviation of the spatial ionospheric gradient (s_{vig}) to LAAS users. Under these normal circumstances, navigation integrity is ensured by incorporating s_{vig} into the computation of position domain protection levels. However, anomalies exhibiting abrupt changes in the ionospheric gradient have been observed during ionospheric storms in October and November 2003. Therefore, monitoring algorithms are necessary for LAAS to detect these hazardous ionospheric anomalies without affecting the system's availability and continuity significantly.

A three parameter (front width, gradient, and front speed) ionospheric threat model has been proposed by Stanford University and significant research has been devoted to the development and analysis of LGF and airborne code-carrier divergence monitors. There are limitations on the effectiveness of these monitors, as they depend on the rate of change of the delay with time. The most hazardous threat in this regard is a static ionospheric wave front and this is the case considered. Two new airborne ionospheric integrity-monitoring algorithms are investigated. The first one uses double difference carrier phase measurements in a Receiver Autonomous Integrity Monitoring (RAIM) type algorithm to detect ionospheric wave fronts. The second one incorporates inertial sensor measurements to address certain regions of the threat space. Ground monitors are also discussed. They are based on detecting the front gradient using the baselines formed by the very precise Integrated Multipath Limiting Antennas (IMLA) already existing in the present LGF configuration. This paper shows wider fronts can be detected regardless of their gradient (within the threat model), and the ideas for dealing with thinner fronts are also presented.

INTRODUCTION

The Federal Aviation Administration is currently developing its Differential GPS (DGPS) type implementation, the Local Area Augmentation System (LAAS) to transition from the current instrument landing system to satellite based navigation. Due to the single frequency nature of the current LAAS architecture, spatial ionospheric decorrelation between the LAAS Ground Facilities antenna and the user contributes significantly to differential ranging errors. During days of normal ionospheric activity, the LGF broadcasts a conservative standard deviation of the spatial ionospheric gradient (s_{vig}) to LAAS users. Under these normal circumstances, navigation integrity is ensured by incorporating σ_{vig} into the computation of position domain protection levels. However, anomalies exhibiting abrupt changes in the ionospheric gradient have been observed during ionospheric storms in October and November 2003. During these occurrences, the ionospheric effect not eliminated by the broadcast range correction can potentially have a magnitude of several meters instead of the nominal millimeter level differences. Therefore, effective monitoring algorithms are necessary for LAAS to detect these hazardous ionospheric anomalies without affecting the system's availability and continuity significantly.

Ionospheric fronts are very difficult to model, as the dynamics of their formation and change with time are not fully understood, and the quantity of data to analyze is limited. Stanford University developed a model that describes the front by its effect (delay) on the signal, and thus allows the front to be defined with only a

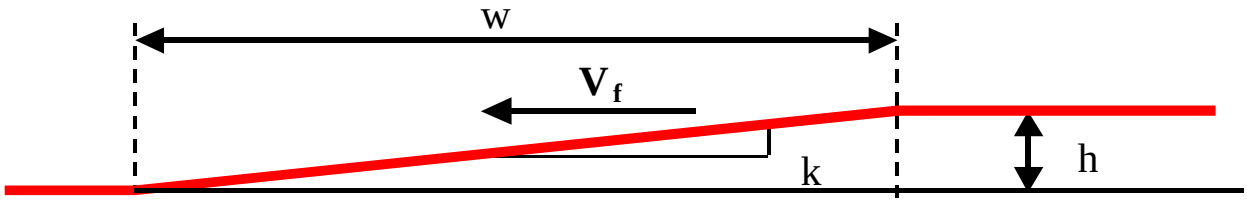

High Elevation /Moving Front	High Elevation /Stationary	Low Elevation (El ≤12°)
W: 25 – 200 km **k: 30 – 500 mm/km** **V_f: 70 – 1000 m/s** ***Max Delay* (h) £ 25 m**	**W: 25 – 200 km** **k: 30 – 250 mm/km** **V_f: 0-70** ***Max Delay* £ 25 m**	**k: 30 – 150 mm/km**

Figure 1: Ionospheric front model and threat space

few parameters, simplifying the analysis [1]. These parameters are the front width (*W*), the front vertical gradient (*k*), the front height (derived from *W* and *k)*, and the front's velocity. By considering the available data from various ionospheric storms, boundaries considered realistic were defined for these parameters, obtaining a threat space. A sketch of the model and the values for the threat space are shown in Fig. 1.

Detection of these types of threats has been studied using ground and airborne variations of the carrier-code divergence monitors. These monitors can mitigate the integrity risk for certain parts of the threat space, but as they depend on the rate of change of the delays, they do not work for slow varying fronts, or stationary fronts.

This work focuses on providing risk mitigation for stationary ionospheric fronts threats, and investigates two basic types of monitors. The first one is airborne, and is a particular implementation of the Residual Autonomous Integrity Monitor (RAIM). The second one is a ground monitor, using baselines between the antennas at the LGF to detect the ionospheric front gradient. The value of integrating inertial information with the GPS measurements is also explored.

The purpose of the monitors analyzed is not to detect an ionospheric storm, but to detect if the storm is affecting a particular runway of an LGF site. The LGF would get a storm warning from WAAS or NASA's STEREO satellite system [1][2]. This means that the availability losses from the monitors presented in this paper might apply only during a storm depending on how they are implemented. The hazardous situation for LAAS is not for the LGF and the user being in a high signal delay zone of a front, but when the delay at the LGF and the user's position is significantly different. This is also why a failure on only one satellite at a time is considered, as the likelihood of two satellites simultaneously being in the border of the area in the sky with big (or low) delay with respect to the LGF is considered negligible. This assumption is coincident with the observed data [3]. The variable *W* considered in this analysis is not the physical width of the front, but the width of the front that lies between the LGF antenna and the aircraft. That is why, even though a physical front smaller than 25 km is not in the threat space, the lower limit *W* analyzed has to be 0. This can be observed in figure 2, where the width is represented by the green line starting at the LGF antenna, even though a part of the front not affecting the approach continues to the left.

DIFFERENTIAL CARRIER PHASE RAIM TYPE MONITOR

This monitor works in two phases. The user makes a geometry screening before initiating the approach. If the geometry passes this test, at the LGF Broadcast Radius distance (x_{BR}) the user will compute a single difference user (A) - LGF (G) carrier phase measurement for each satellite *i*:

$$f_i^{SD0} = f_i^{A0} - f_i^{G0} \quad (1)$$

that will be employed as a reference. As it moves closer to the LGF, it generates a double difference measurement

$$f_i = f_i^{SD} - f_i^{SD0} \quad (2)$$

using a second differential carrier phase measurement; being the Decision Height distance (x_{DH}) the last point to detect a failure. The power of this implementation resides in the use of the very precise carrier phase measurements, and that it uses differential measurements taking advantage of the baseline formed by the airplane as it executes its approach. The values used in the results presented for x_{BR} and x_{DH} are 45 km and 5 km respectively. It must be stated that for the user to be able to compute these differential measurements, the LGF

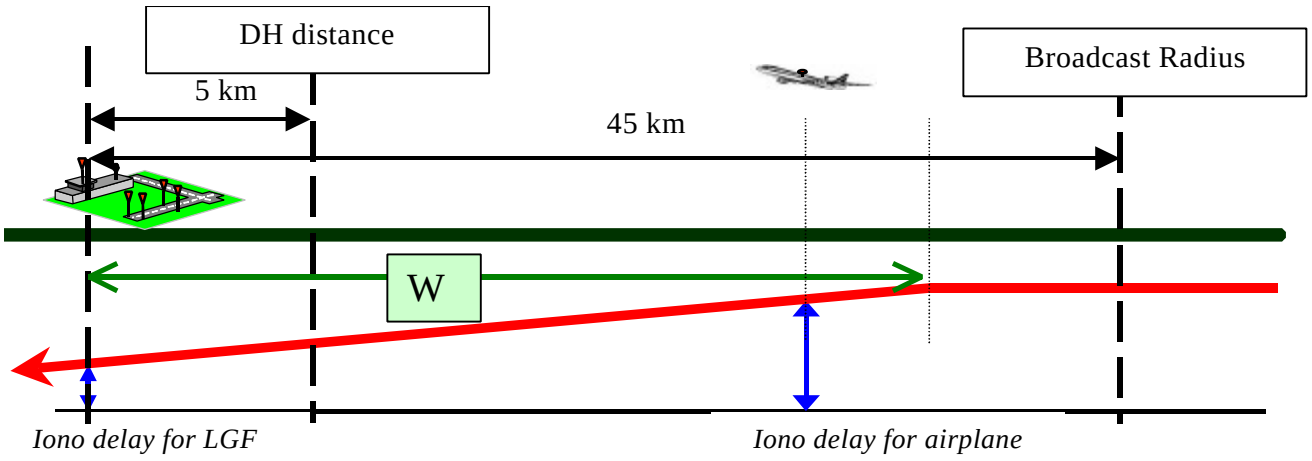

Figure 2: Approach with ionospheric front present.

would need to broadcast carrier phase corrections (LAAS message Type 6).

Using the computed Line Of Sight unit vectors (LOS), the user will obtain a residual vector as:

$$\begin{bmatrix} r_1 \\ r_2 \\ \vdots \\ r_n \end{bmatrix} = \begin{bmatrix} f_1 \\ f_2 \\ \vdots \\ f_n \end{bmatrix} - \begin{bmatrix} -LOS_1 & 1 \\ -LOS_2 & 1 \\ \vdots & \vdots \\ -LOS_n & 1 \end{bmatrix} \begin{bmatrix} \Delta\hat{x} \\ u \end{bmatrix} = f - H\hat{u} \qquad (3)$$

where the differential position vector $\Delta\hat{x}$ (in our case the vector with origin in the airplane's position at x_{BR} and ending in the x_{DH} position), and the clock bias u are obtained from:

$$\hat{u} = (H^T V^{-1} H)^{-1} H^T V^{-1} f \qquad (4)$$

with V being a time (t) changing diagonal weighting matrix whose elements are computed as:

$$\left(s_i^t\right)^2 = 2s_{SD}^2 + \left(s_{vig} \times \Delta z_i^t \times Ob_i^t\right)^2 \qquad (5)$$

where:

s_{SD}, is the single difference carrier phase measurement standard deviation (a nominal value of 1 cm is used in this work);

s_{vig}, is the fault free vertical ionospheric gradient.

Δz, is the distance between the two airplane-SV measurement rays (one at BR and one at DH distance), and

Ob, is the obliquity factor.

The values of Δz will have a maximum of 40 km and vary according to the *Az* and *El*. (Taking this factor into account instead of using a constant value of 40 km has an impact on the final results). The time superscript is dropped from now on.

The test statistic for this monitor will be similar to the one in a Residual Autonomous Integrity Monitor (RAIM) implementation: the norm of the residual vector, now weighted using (5):

$$r = \left\| \begin{bmatrix} \frac{r_1}{s_1} & \frac{r_2}{s_2} & \cdots & \frac{r_n}{s_n} \end{bmatrix} \right\| \qquad (6)$$

Under normal conditions r can be considered to be Chi Square distributed with n-4 degrees of freedom, being n the number of satellites [4].

The results that follow are very sensitive to the assumptions made regarding the constellation and the standard deviation for the measurements used.

In this work the 27 primary slot constellation (based on [5]) was used with an outage model that is conservative with respect to the outage history for GPS.

Several values for s_{vig} were explored as it is the driving parameter for the value of s_i (5), and a nominal value of 2 mm/km was used. Note that if the value selected was not conservative enough, the availability loss and

continuity risks would be higher than the ones from the simulation, but not the integrity risk, as the result of this error will only affect the predicted number of false alarms.

After stating the assumptions made, the purpose of the following sections, is to determine when the availability lost in the geometry screening is tolerable, and for what types of threats (i.e. what combinations of widths and gradients) the monitor is effective.

SLOPE MODIFIER ALPHA

In case of a failure caused by an ionospheric storm, its impact on the test statistic r will be [6]:

$$r^I = \left(I_d - HH^*\right)_{:,i}\left(d_{i(DH)} - d_{i(BR)}\right) \qquad (7)$$

where:

I_d , is the identity matrix

H^* , is the pseudoinverse of H, weighted with matrix V (4) and;

d_i , is the bias introduced in the carrier phase single difference measurement for satellite i by the ionospheric front.

The vertical position error caused by the failure will be:

$$dx_v^I = H_{3,i}^+ f_{i(DH)}^I \qquad (8)$$

where:

H^+ , is the pseudoinverse of H weighted according to the differential carrier smoothed code specifications for LAAS Cat I [7], and

f_i^I , is the error accumulated in the differential Hatch filter measurement to satellite i.

Both effects (on the vertical position error and on the residual) have been considered at decision height distance, as it has the most stringent VAL.

The probability of a Missed-Detection (MD) given a failure (represented generically by F in the formula) is:

$$P_{MD} = P(dx_v > VAL) \times P(r < T) \mid F \qquad (9)$$

where T is a threshold derived from the tolerable probability of a false alarm applied to the corresponding Chi Square distribution.

By first defining a slope modifier "Alpha Iono" as:

$$a_I \equiv \left| \frac{d_{i(DH)} - d_{i(BR)}}{f_{i(DH)}^I} \right| \qquad (10)$$

A Failure Mode Slope (FMS) is defined as:

$$FMS \equiv \frac{\left|dx_v^I\right|}{\left\|r^I\right\|} = \frac{1}{a_I} \frac{\left|H_{3,i}^+\right|}{\left\|\left(I - HH^*\right)_{:,i}\right\|} \frac{f_i^I}{f_i^I} = \frac{1}{a_I} \frac{\left|H_{3,i}^+\right|}{\left\|\left(I - HH^*\right)_{:,i}\right\|} \qquad (11)$$

For each geometry, a plot of vertical error dx_v with respect to the norm of the residual can be generated (Fig. 3), where the slope of a line is defined by the FMS, and the nominal distribution or fault free "noise" is schematically represented by the ellipses. The location along this line where the P_{MD} is the biggest (darker ellipse in the figure) can be obtained. If that P_{MD} is bigger than the integrity threshold (a value of 10^{-4} was used in the simulations) that geometry is discarded. However, if the slope is multiplied by a certain a_I, making the FMS smaller, the geometry might become available as the P_{MD} area becomes smaller. By doing this analysis for all geometries during a whole day, the availability for each site and each value of a_I can be obtained. If a certain tolerable availability is defined (a value of 99.9% was considered desirable in this analysis), the necessary a_I at each site can then be obtained.

The advantage of writing the FMS as in (11), is that it allows a geometry analysis that can momentarily ignore the nature of a_I. After the availability issue is addressed, the meaning of a_I will determine what types of threats can be detected with this monitor implementation. This will become more obvious to the reader in the following section.

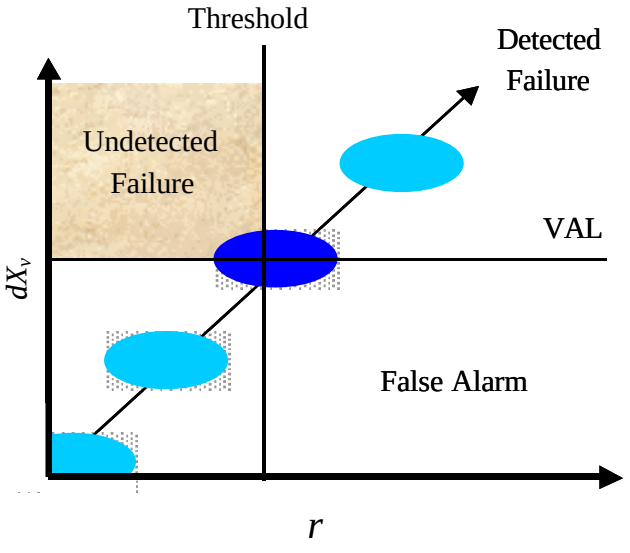

Figure 3: FMS and P_{MD}

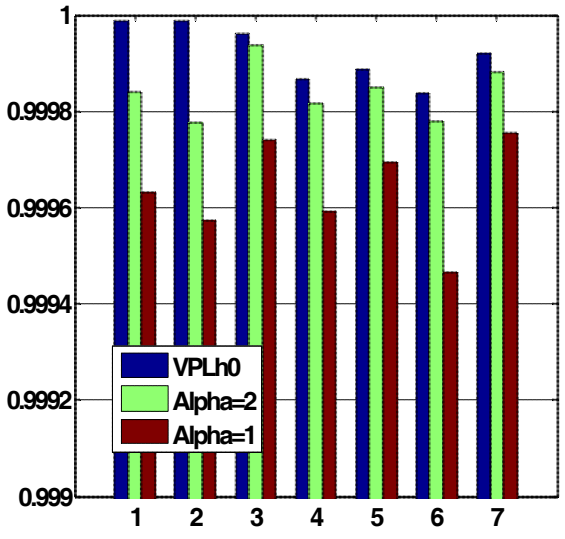

a. s_{vig}= 2 mm/km

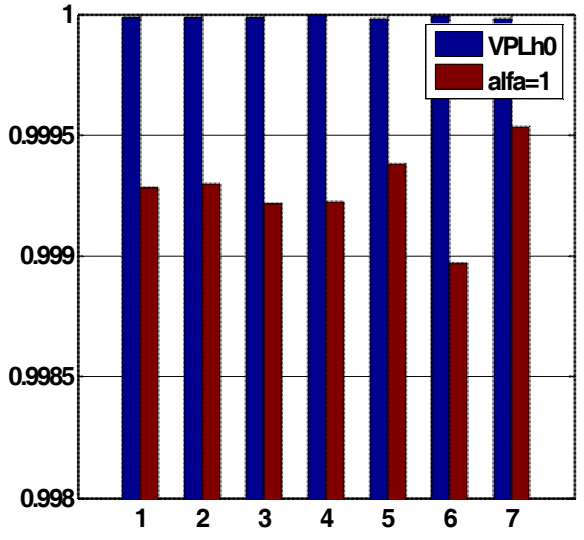

b. s_{vig}= 3 mm/km

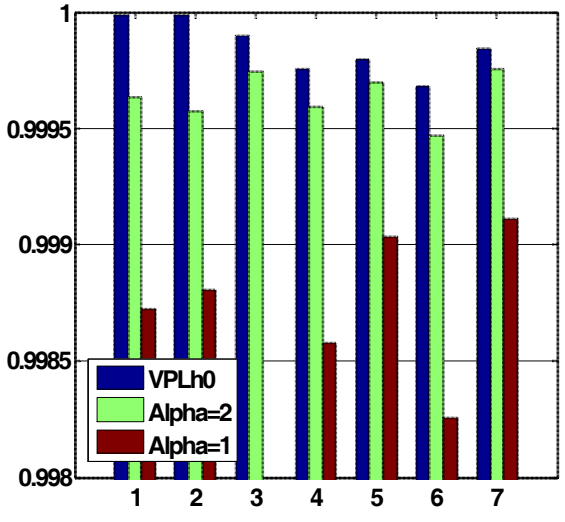

c. s_{vig}= 4 mm/km

LOCATIONS

1. Chicago
2. Dallas
3. Cambridge Bay
4. Los Angeles
5. Seattle
6. New York
7. Miami

Figure 4: Availability for different values of a_I

The results in figure 4 show that, if the nominal parameter values of our model are used, a value of $a_I = 1$ has a tolerable availability loss for the 7 sites considered. If a model with s_{vig} =4mm/km is used instead, $a_I = 2$ will be sufficient. That means that all ionospheric storms whose effects on the carrier phase and carrier smoothed code measurements give a value that is smaller than a_I when related according to (10), can be detected meeting the integrity and availability risks defined $\left(P_{MD} < 10^{-4}; P_{ffa} < 10^{-7}\right)$. Which fronts satisfy (10) for these values of a_I is the subject of the following section.

WIDE FRONT DETECTION

The error accumulated in the Hatch filter at time epoch q given by the storm will be [6]:

$$f_{(q)}^{I} = \left(\frac{N-1}{N}\right)^{q} f_{(0)} + \sum_{j=1}^{q}\left(\frac{N-1}{N}\right)^{j}\left[d_{(q+1-j)} - d_{(q-1)}\right] + \sum_{j=1}^{q}\left(\frac{1}{N}\right)\left(\frac{N-1}{N}\right)^{j-1}\left(-d_{(q+1-j)}\right) \quad (12)$$

were:

$$N = \frac{t}{\Delta t} = \frac{100s}{0.5s} = 200 \qquad (13)$$

with t being the filter time constant, and Δt the interval between each measurement.

Considering the storm model described in Fig. 1 the inputs for (12) will be:

$$f_{(0)} = h = w \times k \qquad (14)$$

$$d = h - k \times v \times t \qquad (15)$$

where t is the time from the moment the airplane reaches the changing part of the front , and v is the aircraft speed (Fig. 2).

A continuous version of the ionospheric filter error, taken at x_{DH} is:

$$f^{I} = k\left[x_{DH} + 2vt\left(1 - e^{-\frac{w - x_{DH}}{vt}}\right)\right] \qquad (16)$$

Formula 10 can now be written as:

$$a_I = \frac{k(w - x_{DH})}{k\left[x_{DH} + 2vt\left(1 - e^{-\frac{w - x_{DH}}{vt}}\right)\right]} \qquad (17)$$

where the numerator should be replaced by 0 if the front is thinner than x_{DH} (the ionospheric effect on the measurement at x_{BR} and the measurement at x_{DH} will be the same, so there is no detection capability), and by $k(x_{BR} - x_{DH})$ if the front is wider than x_{BR} (the single difference reference measurement (1) cannot be obtained outside the broadcast radius).

Note the k's in the numerator and denominator cancel each other, so the gradient does not affect the FMS.

Figure 5 shows the values of a_I with respect to the front width. It is clear from the plot that if an $a_I = 1$ is tolerable in the geometry screening (such is the case for the 7 sites considered, Fig 4.a.), any front wider than 22.9 km is detectable regardless of the front's gradient. (Recall in the availability analysis, the position with the biggest P_{MD} was considered for each geometry (Fig. 3), so no k can give a P_{MD} bigger than the one obtained then). If a site requires an $a_I = 2$, any front wider than 42.8 km can be detected.

THINNER FRONT DETECTION

To detect thinner fronts, the simulations take extensive time, as each combination of width and gradient has to be evaluated (the convenience of using a_I is lost). Some general ideas and preliminary results follow.

The first case analyzed is a front with a width equivalent to x_{DH} (for these studies, 5 km). That is the widest front for which the RAIM type monitor has no detection capabilities at all. Thus, the only part of the monitor working would be the geometry screening, in which a geometry is considered to be unavailable if the $P_{MD} = P(dx_v > VAL) \mid F(w = 5km)$ is bigger than 10^{-4}.

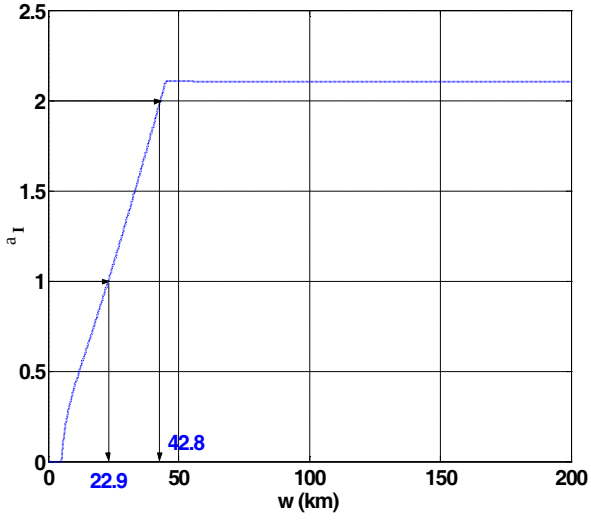

Figure 5: a_I with respect to front widths

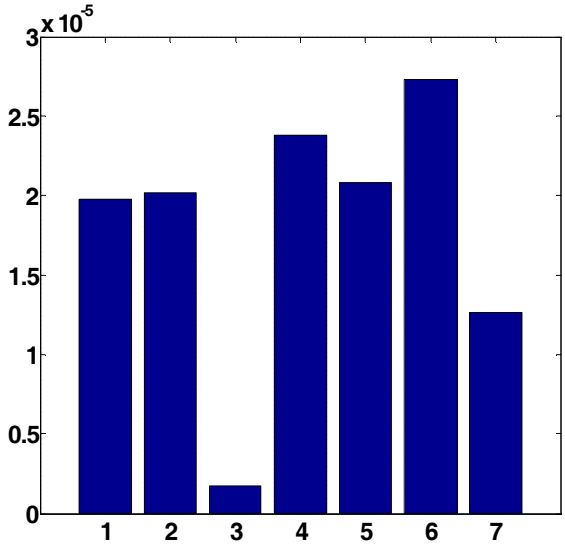

Figure 6: Availability loss for 5km front geometry screening (see Fig. 4 for locations).

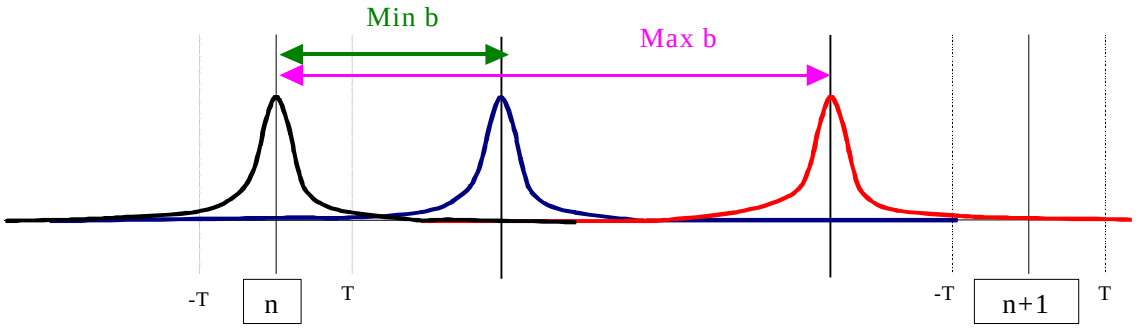

Figure 7: LGF baseline monitor test statistic

Figure 6 shows that the availability loss with respect to the VPH_0 availability is tolerable.
For fronts wider than x_{DH}, the availability loss for certain combinations of w and k will still be tolerable. This work is in process.

LGF DETECTION

The threat model considers that physical fronts are at least 25 km wide. As the fronts not dealt with using the carrier phase based RAIM have a maximum extension of 22.9 km, at least 2.1 km of the physical front will be between x_{DH} and the LGF, so it is relevant to explore the detection capabilities at the LGF.

The basic idea is to use the Integrated Multipath Limiting Antennas (IMLA) existing in the present LGF configuration. With them, baselines can be formed, and by taking differential measurements the gradient of the front can potentially be detected. This takes advantage of the great precision of these antennas, considered to be approximately 3 mm standard deviation for a double difference measurement [8].

A monitor idea was introduced in [8] that used a triple difference measurement test statistic (to remove the cycle ambiguity), that could detect gradients bigger than 150 mm/km with a 100 m baseline, and all gradients with a baseline that was 500 m long. However, this monitor would not work if the storm was already present when the satellite rises. A suggestion to deal with this problem was to consider elevating the mask during an ionospheric storm warning, to ensure the reference measurement was outside the storm (in other words to make sure the pierce points of the initial and final measurements were at least 200 km apart).

A different implementation is described in this section. It also uses baselines between the existing antennas, but its test statistic is based on integer ambiguity estimation (thus avoiding the triple difference). The test statistic S for this monitor is the difference between the estimate of the cycle ambiguity and the closest integer n:

$$S = \hat{C}_{Amb} - n = N(0, s) \qquad (18)$$

The distribution of S is normal, and is represented by the black curve in Fig. 7. In case of a storm causing a bias b in the measurement, the distribution of S will be:

$$S = N(b, s) \qquad (19)$$

A threshold T is set to satisfy the continuity specification for the system. If b is bigger than a certain magnitude, the P_{MD} (when $S < T$) will become small enough to consider it detectable, thus giving a minimum detectable bias. This case is represented by the blue curve giving the distribution, and the green line showing the minimum b. As the error becomes bigger the area under the right tail past $-T$ (for the n+1 integer) will be big enough to make the P_{MD} bigger than the integrity risk allowed, determining a maximum detectable bias. This is represented by the red distribution and the pink bias magnitude in the figure 7.

Figure 8 shows the detectable slant delays with respect to baseline length (X_{bl}), with a different pair of curves corresponding to each value of s. The top and bottom horizontal lines represent the maximum and minimum slant gradients for the threat space. The formulas corresponding to minimum and maximum detectable gradients are:

$$k_{MAX} = \frac{0.19\,cm - (K_{ffa} + K_{MD})s}{X_{bl}} \qquad (20)$$

$$k_{MIN} = \frac{(K_{ffa} + K_{MD})s}{X_{bl}} \qquad (21)$$

with the K's being the multipliers corresponding to the fault free alarm and MD specifications.

For each combination of baseline length (between LGF antennas) and s, a range of detectable gradients can be extracted from the plot. The left vertical line shows that for a baseline of 220m, all gradients bigger than 180 mm/km can be detected with a s of 3 mm. The second vertical line shows that for a baseline length of 400m, any gradient between 120 and 380 mm/km can be detected

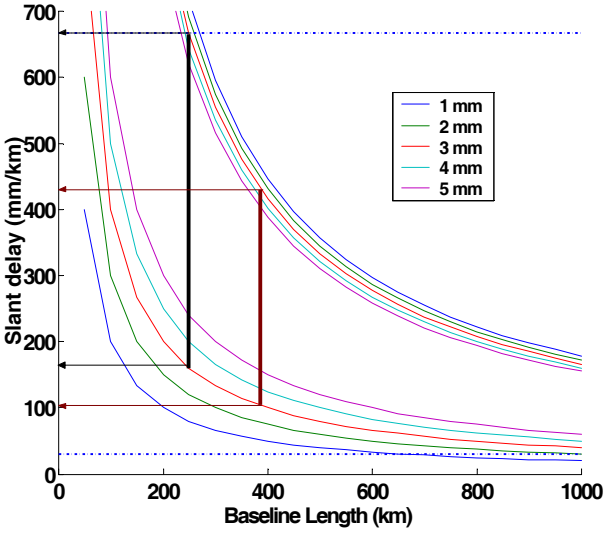

Figure 8: Maximum and minimum detectable gradients for LGF monitor

with the same sigma in the double difference measurements.

INERTIAL-GPS INTEGRATION

Another possibility to mitigate integrity risk for the thinner fronts is to integrate INS information with the carrier phase RAIM described in previous sections. This approach is studied in this section.

A simplified INS model has been selected due to the short application interval (less than 4 hr). [9]. Figure 9 shows an example (east channel) block diagram of the simplified INS model.

The covariance analysis is implemented using the INS model to simulate the propagation errors. [10],[11] The simulated result of INS coasting errors is shown on figure 10.

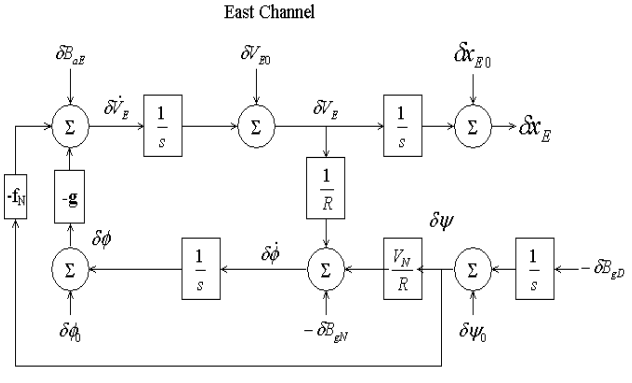

Figure 9: Simplified INS model (East channel)

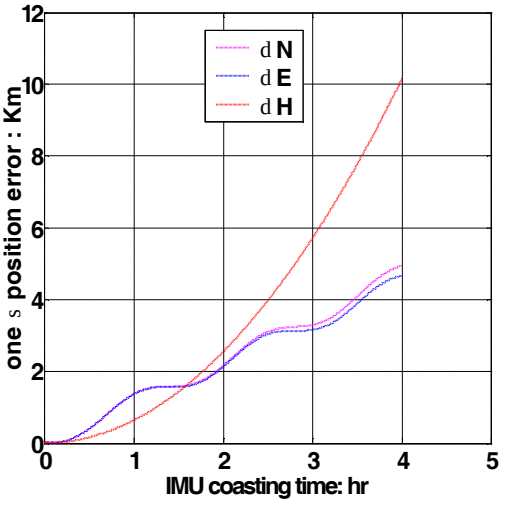

Figure 10: Simulated INS coasting errors

The very low noise of GPS carrier phase measurements and the small INS position propagation errors during short periods are two key elements in the algorithms of INS/GPS integration to detect ionospheric storms.

INS AIDED CARRIER PHASE RAIM DETECTION

Two single difference carrier-phase GPS measurements between the aircraft and the LGF, separated by INS coasting interval *Dt* are generated after the aircraft enters the LAAS service volume:

$$f^{SD}_{i(t_0)} = -LOS_{i(t_0)} \cdot x_{(t_0)} + u_{t_0} + N_i - I_i + T + n_{f^{SD}} \qquad (22)$$

$$f^{SD}_{i(t_1)} = -LOS_{i(t_1)} \cdot x_{(t_1)} + u_{t_1} + N_i - I_i + T + n_{f^{SD}} \qquad (23)$$

where $t_1 = t_0 + Dt$, $x_{(t)}$ is the relative position vector from LGF to aircraft, u is the clock bias between the two receivers, N represents the cycle ambiguity, and I and T are the nominal ionospheric and tropospheric errors respectively.

A double difference carrier-phase GPS measurement can be formed by subtracting eq (22) from eq (23):

$$f = -LOS_i \cdot \Delta x + u + n_{f+dI} \qquad (24)$$

An estimate of the vector *Dx* is available using the aircraft position propagations obtained from INS during this coasting interval *Dt*.

$$\Delta \hat{x} = I_d \, \Delta x + v_{\Delta \hat{x}} \qquad (25)$$

All available double difference carrier-phase GPS and INS measurements can be stacked together in matrix form:

$$\begin{bmatrix} f_1 \\ \vdots \\ f_n \\ \Delta\hat{x} \end{bmatrix} = \begin{bmatrix} -LOS_1 & 1 \\ \vdots & \vdots \\ -LOS_n & 1 \\ I_d & 0 \end{bmatrix} \begin{bmatrix} \Delta x \\ u \end{bmatrix} + \begin{bmatrix} n_1 \\ \vdots \\ n_n \\ n_{\Delta\hat{x}} \end{bmatrix} \quad (26)$$

Now the monitoring process initiated in (3) can be done with the added information from the INS measurements.

The performance of the detection algorithms is sensitive to aircraft coasting interval. When the coasting interval increases, the observed ionospherical spatial decorrelation error increase, making it easier to detect. On the other hand the INS propagation errors increases as well degrading the detection performance. The optimal resolution of this tradeoff is currently being investigated..

Initial results suggest the coasting distances needed for detection are less than 4 km, allowing detection of the higher values of *k* regardless of the fronts width. This would allow mitigating a portion of the threat space with thinner fronts.

CONCLUSIONS

In this paper risk mitigation options were explored for LAAS against static ionospheric fronts. A Residual Autonomous Integrity Monitoring (RAIM) algorithm using differential carrier phase measurements was described. It was demonstrated that if used in combination with a geometry screening before initiating the approach, all fronts thinner than 5 km or wider than 22.9 km can be detected regardless of their gradient. The implementation of this monitor would result in a tolerable availability loss, and require the broadcast of LAAS message Type 6 (carrier measurement corrections). The detection capabilities of the LAAS Ground Facility using antennae baselines to detect front gradients was explored showing results for different measurement quality and baseline lengths. Preliminary algorithms for using INS aided carrier phase RAIM were also investigated.

ACKNOWLEDGMENTS

The authors wish to acknowledge Sam Pullen and Ming Luo for their useful comments on the threat model and the specifications to be used, and the Federal Aviation Administration for sponsoring this research.

REFERENCES

[1] Luo, Ming, L., Pullen, S., Walter, T., and Enge, P., "Ionosphere Spatial Gradient Threat for LAAS: Mitigation and Tolerable Threat Space", *Institute of Navigation's National Technical Meeting*, San Diego CA 2004

[2] "*The Sun and The Heliosphere in Three Dimensions*", Report of the NASA Science Definition Team for the STEREO Mission, 1997

[3] Private conversation with Dr. Sam Pullen , October, 2004

[4] Pervan, B., "*Navigation Integrity for Aircraft Precision Landing using the Global Position Landing*" Ph.D. Thesis, Dept. of Aeronautics and Astronautics, Stanford University, Stanford, March 1996

[5] Massatt, P, et. al. "Assessment of the proposed GPS 27-Satellite Constellation" *ION GPS/GNSS*, Portland, OR, September 2003

[6] Andreacchi, J., "*Characterizing the Effect of Ionospheric Divergence on Differential GPS Navigation*" M.S. Thesis, Dept. of Mechanical, Materials, and Aerospace Engineering, Illinois Institute of Technology, Chicago, July 2000

[7] "*Minimum Aviation System Performance Standards for the Local Area Augmentation System*" RTCA Paper No.037-98/SC159-778, February 1998

[8] Gratton, L., et.al, "Experimental Observations and Ephemeris Monitor Applications of LAAS Carrier Phase IMLA Measurements", *Institute of Navigation's GNSS meeting*, Long Beach, CA, September 2004

[9] D. H. Titterton, J.L. Weston, *Strapdown Inertial Navigation technology*, Peter Peregrinus Ltd., on behalf of the Institution of Electrical Engineers, London, United Kingdom, 1997.

[10] D. Gebre-Egziabher, *Design And Performance Analysis of A Low-cost Aided Dead Reckoning Navigator*, a Ph.D. dissertation, Stanford University, December 2001.

[11] R. G. Brown, and P. Y.C. Hwang, *Introduction to Random Signals and Applied Kalman Filtering*, J. Wiley & Sons, New York, 3rd edition, 1997.